Long-term thermal stability of TianQin satellites

Dong Wang and Xuefeng Zhang*

MOE Key Laboratory of TianQin Mission, TianQin Research Center for Gravitational Physics and School of Physics and Astronomy and Frontiers Science Center for TianQin, Gravitational Wave Research Center of CNSA, Sun Yat-sen University (Zhuhai Campus), Zhuhai 519082, China

Lihua Zhang† and Ming Li‡

DFH Satellite Co. Ltd., CAST, Beijing 100094, China

(Received 3 November 2023; accepted 15 April 2024; published 13 May 2024)

TianQin is a proposed space-based gravitational wave detection mission featuring high geocentric orbits. The strain sensitivity goal imposes stringent requirements on thermal control of the key science payloads, which relies heavily on the support of the satellite platforms. A main challenge for TianQin is the yearly varying sunlight directions with respect to the constellation plane. It leads to significant variations in the external heat flow, which is unfavorable for maintaining stable working temperatures inside the satellites over the long term. Based on a flattop sunshield design for the satellites and following passive thermal control guidelines, we propose a combined usage of multiple insulation materials, including polyimide foams and aerogel, at the sunshield and top plate of the satellite to enhance the thermal decoupling. The simulation shows that the temperature variation at the key payload bay can be suppressed within ± 0.7 K over three months, which is partly due to the lowered sunshield temperature by employing large areas of optical solar reflectors. Additionally, the design is also effective in damping down the thermal noise from the solar constant fluctuations in the mHz frequency band. The results can provide useful environmental input for studying temperature-related effects on the science payload performance.

DOI: 10.1103/PhysRevD.109.102007

I. INTRODUCTION

The TianQin mission plans to deploy a constellation of three satellites at an altitude of $\sim 10^5$ km in high Earth orbits, and to form a giant triangle-shaped laser interferometer for detecting gravitational waves (GWs) in the frequency band of 0.1 mHz to 1 Hz [1]. In the detection band, stringent requirements are placed on the residual acceleration noise of test masses (TMs) at 1 $\mathrm{fm/s^2/Hz^{1/2}}$ level and on the TM-to-TM displacement measurement noise at 1 $\mathrm{pm/Hz^{1/2}}$ level. These top-level requirements call for ultrastable and ultraquiet performance from the satellite platforms. Notably, the thermal stability of the key payload—consisting of telescope, optical bench, and inertial sensor—poses a great challenge to the satellite thermal control, demanding $\sim 5\ \mu\mathrm{K/Hz^{1/2}}$ at the inertial sensors (also known as gravitational reference sensors) and optical benches in the detection band [1].

Compared to heliocentric space-based GW detection missions represented by LISA [2], the geocentric design of TianQin has benefits in terms of launch and deployment, guidance and navigation, data communication, etc. One of the main challenges is the negative impact of sunlight variations on the intersatellite laser links and the satellite thermal control. Thus, a preliminary "$3 + 3$ months" operational concept was proposed [1], i.e., that the science observation of GWs is suspended when the incoming sunlight is roughly parallel with the constellation plane (see Fig. 1). The mission is expected to last five years.

Based on experience from other missions such as LISA [4], GAIA [5], and WMAP [6], TianQin has adopted a single flattop sunshield in the satellite design [3,7], so that the external heat flow impinging on the satellites can be made more stable with the key payloads, including telescope openings, always kept in the shade. The research conducted on the TianQin thermal control has focused on modeling and analyzing the in-orbit thermal environment [8–10]. Notably, TianQin experiences significant variations in the solar heat flow, which range from 960 $\mathrm{W/m^2}$ to 1314 $\mathrm{W/m^2}$ during one 3-month observation window (38.5% over three months). This is a special challenge to TianQin when compared with LISA, which has $\sim 4\%$ fluctuation over one year. Meanwhile, in the target frequency band of 0.1 mHz to 1 Hz, the external heat flow variation due to the solar constant fluctuation (SCF) is

*zhangxf38@sysu.edu.cn
†zlh70717@sina.com
‡dawn75918@126.com

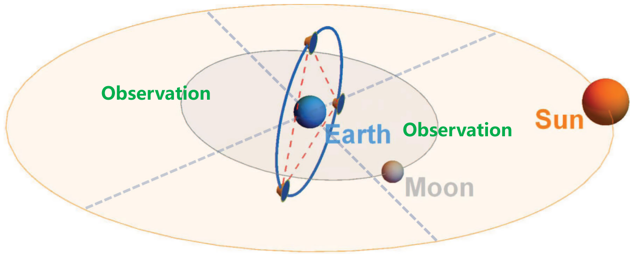

FIG. 1. Illustration of the TianQin constellation in an Earth-centered reference frame (not to scale) [3]. As the normal of the constellation plane points to the reference GW source RX J0806.3 + 1527, the incoming sunlight direction has a yearly variation relative to the constellation plane.

$\sim$5 $\mathrm{W/m^2/Hz^{1/2}}$ for TianQin, which is at the same level of LISA [8]. The work of [9] has analyzed the differences in the external heat flows among the three TianQin satellites and discussed their possible impact on the satellite temperatures. In addition, the Ref. [10] has introduced an analytical approach for investigating the sunshield's temperature response to sinusoidal fluctuations in the incoming heat flow.

Satellites for space-based GW detection differ from conventional ones by putting emphasis on temperature fluctuations in the detection frequency band. However, in the case of TianQin, the issue of long-term temperature variations inside the satellites caused by the changing external heat flow should also be investigated. This is owing to that several aspects of the payload functioning such as laser frequency stabilization, tilt-to-length coupling [11], and self-gravity variation, also associate with long-term thermal stability outside the measurement band. Though the specific requirements are still being studied, it is generally considered desirable to have long-term thermal stability for TianQin, which was somewhat overlooked in the past.

To add more difficulty, TianQin aims to address this challenge by employing a passive thermal control design that prevents unwanted interference to science measurements. Therefore, the use of thermal switches, heat pipes, and devices with moving parts is avoided for the science operation [12,13]. These limitations may complex TianQin's thermal control, and solving the issue relies heavily on system-level design, insulation material properties, etc.

Lessons can be learned from the LISA and LISA Pathfinder (LPF) missions. For LISA, an initial satellite design was proposed in 2000, laying a groundwork for structure and thermal, and self-gravity analyses [4,14,15]. In 2009, polyimide foams, low emissivity coatings, etc. were used in the solar heat flow transfer path, and the multistage passive thermal insulation was planned to avoid thermal disturbances affecting key payloads [16]. Thermal simulation results indicated that the temperatures at the optical benches were close to room temperatures, and the required stability could be achieved without active temperature control. The temperature fluctuations caused by solar input at 1 mHz were approximately 2×10^{-9} $\mathrm{K/Hz^{1/2}}$ at the optical benches.

The LPF, a technology demonstration mission for LISA, was launched in 2015 and positioned around the Lagrange Point L1 [17,18]. The optical bench exhibited a temperature stability of 3×10^{-5} $\mathrm{K/Hz^{1/2}}$ at 0.1 mHz, and the sunshield maintained a temperature around 112 °C with only a 0.4 °C variation over six days [12,13,19]. The exceptional thermal stability of the LPF in orbit relies not only on a stable thermal environment in its orbit but also on careful implementation of passive thermal control. LISA's thermal design is likely to inherit that of LPF [2,20]. For a quick reference, the thermal control status is summarized in Table I from different LISA models and the LPF in-orbit results. Other related studies can be found in, e.g., [21,22].

The thermal control of the LISA spacecraft has undergone design iterations from the initial stage to the current phase of the mission and followed passive thermal design guidelines. Both computational analysis and in-orbit validation by LPF have demonstrated that the passive thermal

TABLE I. Summary of LISA/LPF thermal control.

Parameter	Location	Value	Reference
Operating temperature	Laser unit	23–29 °C	LISA-2017 [20]
	Optical bench	10–30 °C	
	Telescope	−100–30 °C	
	Gravitational reference sensor	0–30 °C	
Temperature stability	Solar array	50 $\mathrm{mK/Hz^{1/2}}$ at 1 mHz	LISA-2009 [16][a]
	Top plate	5 $\mathrm{mK/Hz^{1/2}}$ at 1 mHz	
	Bottom plate	10^{-5} $\mathrm{K/Hz^{1/2}}$ at 1 mHz	
	Payload shield	5×10^{-6} $\mathrm{K/Hz^{1/2}}$ at 1 mHz	
	Central cylinder cage	10^{-3} $\mathrm{K/Hz^{1/2}}$ at 1 mHz	LPF [12,19]
	Optical bench	3×10^{-5} $\mathrm{K/Hz^{1/2}}$ at 0.1 mHz	

[a]Stabilities due to solar flux alone.

design can effectively meet the requirements. Similarly for TianQin, passive thermal design principles have been adopted to address the challenges. But note that LISA and LPF differ significantly from TianQin particularly in long-term external heat flow. Specifically, LPF was positioned at the L1 Lagrange point of the Earth and the Sun, while LISA will follow Sun-orbiting trajectories. In both cases, the spacecraft attitudes can be arranged to stabilize the incoming solar flux. Additionally, the LPF core payload does not include telescopes and hence, is not directly exposed to outer space. So the thermal design and results of LPF and LISA can only provide limited reference to TianQin. TianQin's design must incorporate its own characteristics and specific requirements.

In this paper, a preliminary thermal modeling of the TianQin satellites is carried out with input from the thermal environment and orbits. The detailed design of the sunshield is described, and the simulation results are analyzed and discussed.

II. TIANQIN THERMAL DESIGN

Due to extremely weak GW signals, the highly sensitive science payloads impose strong limitations on usable thermal control methods. The TianQin satellites require a special thermal design to target the specific needs.

A. Guidelines for thermal design

The primary objective is to achieve highly stable and passive thermal control of the key payload by managing the balance between absorbed solar heat, internal power consumption, and radiative dissipation. This balance ensures that the instruments operate within desired temperature ranges. The thermal design should adhere to the following guidelines.

(1) The satellite platform should achieve its requirements through passive means, and avoid using heater switches in the science mode, since thermal shocks caused by heater switches can interfere with the science measurement.
(2) Heat pipes should be avoided due to unpredictable liquid movement through the pipes, as it may change the satellite's self gravity to the TMs, which are difficult to compensate. In addition, the vibrations generated by the liquid movement may also disturb the measurements.
(3) Movable parts such as louvers and deployable solar arrays should not be employed to prevent vibrations that may interfere with the science measurements.
(4) The onboard instruments should work in continuous and stable power consumption without switching on and off in the science mode.
(5) The sunshield is expected to play a crucial role in providing shade to the science payloads and insulation from the solar flux noise.
(6) The key payloads should be kept in an environment with suitable temperatures and minimal thermal disturbances. Multiple layers of insulation are expected to achieve thermal decoupling from the surrounding environment.

B. Preliminary satellite model

The thermal guidelines should be incorporated in designing the satellites, and a conceptual model is given in Fig. 2 (for illustrative and evaluation purposes only, not reflecting the final design). The nondeployable flat hexagonal sunshield, with solar arrays on top, is body-mounted to the top plate of the satellite with low conductive supports and a 30 mm gap. To accommodate the key payloads and meet the shading requirements for at least three months of continuous observation, the sunshield has an outer diameter of 4.8 m, covering an area of approximately 15 m^2 with solar arrays occupying 8.8 m^2. The height of the satellite is 0.6 m.

The lower plot of Fig. 2 shows the layout of the satellite with a central cylinder, shear walls, and side panels. The key payload enclosure with two protruding telescope barrels is housed inside the V-shaped key payload bay. The compartmentalization can help with thermal decoupling from the electronic boxes, which are mounted on the shear walls and side panels. In the absence of heat pipes, units with high power consumption, such as the integrated

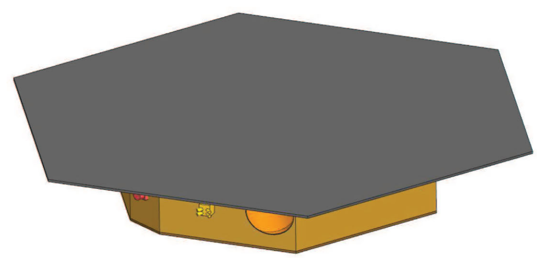

(a) Overall layout

(b) Internal layout with the sunshield and top plate removed

FIG. 2. Test model of TianQin satellites (a, key payload enclosure; b, integrated electronic unit; c, laser unit; ★, test point on the key payload bay).

electronic unit, are positioned on the side panels with dedicated radiator areas facing outer space.

C. Main challenges

The thermal control of TianQin needs to take into account both thermal noises in the frequency domain and operating temperature ranges in the time domain. This section briefly reviews the main challenges in the thermal design.

1. In-band thermal noise

Space-based GW detectors impose stringent requirements on thermal noises within the detection frequency band. Among various disturbances encountered, solar heat flux emerges as an important noise source. Previous studies [7,8] have revealed that the SCF affects TianQin in a similar way as LISA, with the slow changes in the β angle having little impact on solar thermal noise inside the measurement band.

Solar thermal noise can penetrate into the satellite through the sunshield and top plate, thus impacting the key payloads. Moreover, electronic units inside the satellite, such as the front-end electronics of the inertial sensors, the power control and distribution unit (PCDU), and the onboard computers, can also cause thermal disturbances. In order to reduce the impact, a high thermal resistance at the key payload interface and a compartmentalized satellite design are viable measures. Additionally, the satellite's thermal capacity can act as a low-pass filter to attenuate higher frequency noises, which may also be considered in the thermal design.

2. Long-term temperature variation

Variation in solar heat flow caused by the changing β angle poses an additional challenge for TianQin, as it may lead to greater long-term variations in the operating temperatures of the science payloads inside the satellite. Temperature related effects are prevailing in space-based GW detectors, e.g., though structural deformation and optical misalignment. Maintaining high performance of the science payloads may put limits on the operating temperatures. For instance, the laser system should work at zero-thermal-expansion temperatures, of which the allowed range may be of only a few degrees or less (e.g., 23 °C to 29 °C). The specific requirements in this regard are currently being worked out. Nevertheless, we consider it quite desirable, if not mandatory, to have long-term thermal stability for the TianQin satellites as well.

The study aims to address this special challenge of long-term thermal stability. To mitigate the impact of the varying external heat flow, thermal designs with increased resistance and heat capacity at the sunshield and top plate of the satellite are anticipated. The layout and power dissipation of onboard equipment also are important factors, warranting careful design of the radiators.

3. Other challenges

TianQin has opted for body-mounted solar arrays, and the large swing in the β angle during 3-month observation windows results in energy surplus from the power subsystem particularly at the beginning of life (BOL) and large β angles. This surplus has an impact on the temperature variations and is taken into account in our simulations.

To keep the solar array illuminated, the satellites will have to perform attitude maneuvers by flipping 180° when transitioning from one observation window to the next (see Fig. 1). This may disrupt the thermal steady states of the satellites, which should draw attentions from mission operations.

The issue of encountering eclipses during 3-month observation windows has been resolved by eclipse-free orbit design using synodic resonance [3]. There are also possible effects of the Earth and Moon's albedo and thermal radiation on the telescopes, as the latter have direct openings to outer space and point at the distant satellites. The issue is currently under investigation and the design solution will be reported elsewhere.

D. Preliminary thermal design

The thermal insulation of the TianQin satellites consists of multiple stages towards the key payload, including the sunshield, the top plate, the V-shaped key payload bay, and the key payload enclosure (see Fig. 2).

To handle highly variable thermal environments, typical thermal control techniques include active heating [23,24], passive insulation, thermal coatings, louvers [25,26], radiators, etc. However, as far as TianQin is concerned, passive measures are preferred, such as polyimide foams [27–29], aerogels [30,31], multilayer insulation (MLI) [32,33], and low absorption/emissivity coatings. This section describes the thermal design in more details.

1. Sunshield

Acting as the primary barrier against the solar heating, the sunshield necessitates a customized design to mitigate the impact of changing external heat flow. The amount of absorbed solar heat is related to the thermo-optic properties of the materials on the illuminated surface of the sunshield. To prevent direct sunlight onto the satellite's side panels and telescope openings for at least three months, a large sunshield is required (4.8 m in diameter). The unoccupied areas between solar cells are to be covered by low-absorbance optical solar reflectors (OSRs) [34,35]. The arrangement of solar cells and OSRs should be well spread to prevent large temperature gradients across the sunshield. The detailed layout is out of the current scope, and instead

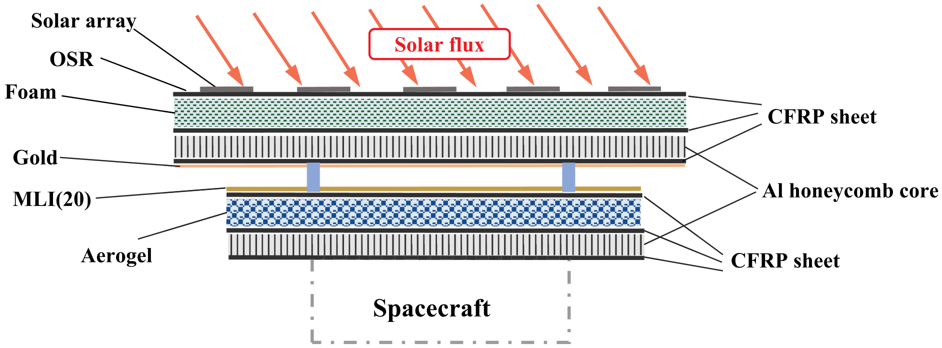

FIG. 3. Illustration of thermal design of TianQin sunshield and top plate.

the area-averaged material properties are used in the simulation.

In the case of TianQin, about 8.8 m^2 of the 15 m^2 sunshield is needed for solar cells, resulting in a less coverage of 59%. This permits significant open areas to lay OSRs. Given these areas, the overall absorptivity of the TianQin sunshield is estimated to be 0.398. It helps lower the sunshield temperature and the temperature variations though radiative transfer to the satellite body (radiative transfer dependent on T^4), which can be beneficial to TianQin.

The sunshield is given a multilayered design, as shown in Fig. 3. The shield consists of 20 mm thick polyimide foams and a 20 mm thick sandwich plate, and the latter is made of carbon fiber reinforced plastic (CFRP) face sheets and an Al honeycomb core. The combination serves dual purposes of thermal insulation and rigid support. Polyimide foams, with advantages in lightness, low conductivity, and shock absorbance, are the main contributor to the solar heat insulation for TianQin, and have been used in other missions with high thermal stability requirements [36].

Both the sunshield and the top plate play important roles in cutting off the solar heat transfer. The top plate consists of 20 mm thick aerogel and a 20 mm thick sandwich plate, and is covered by 20 layers of MLI. Aerogel is selected for its availability and lightness. The combined use of several insulation materials not only lowers the overall temperature level, but also help reduce the temperature variations. The subsequent section will provide an account of the performance of this design.

2. Satellite platform

For the bottom side of the top plate, gold coating with a 0.05 emissivity is applied (see Fig. 4). To reject waste heat, the mounting interfaces of the electronic boxes are enhanced with a conductive filler. The internally facing surfaces of the side panels and shear walls are coated with high emissivity black paint to even out temperatures. The telescope shield is covered by gold coating both internally and externally to minimize thermal disturbance to the barrels.

Radiators are located at the side and bottom plates near high-power devices and are coated with high emissivity white paint. Areas of the external surfaces that do not serve as radiators are covered with MLI to provide insulation and to reduce heat loss.

E. Finite element simulation

The study utilizes the NX 3D Space Systems Thermal Module and the MSC Thermica to conduct thermal analysis of the test model. The sunshield is exposed to a

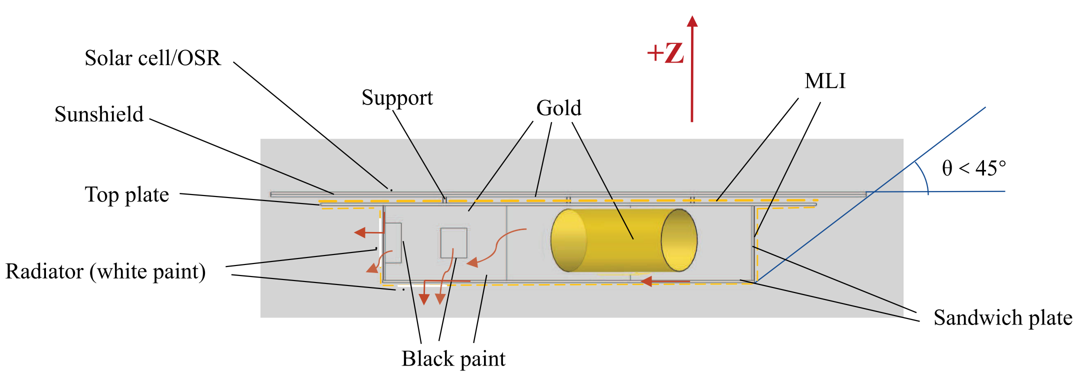

FIG. 4. Illustration of thermal design of TianQin satellite platforms.

TABLE II. MLI thermal properties.

Number of layers	Equivalent emissivity
10	0.017
20	0.016

TABLE III. Thermal parameters of insulation materials.

Materials	Thermal conductivity [W/(m K)]	Density (kg/m^3)	Heat capacity [J/(kg·K)]
CFRP sheet	10	1700	1000
Polyimide foam	0.0054	50	1050
Aerogel	0.02	30	600

precalculated external heat flow based on numerical orbits, while the internal equipment generates approximately 670 W of heat dissipation in the science mode. The sunshield, top/bottom plates, side panels, shear walls, central cylinder, key payload enclosure, and electronic boxes are created with regular geometric shapes. Then, these models are meshed with input of material and surface properties, and contact conditions are imposed. Numerical simulations are performed for 3-month observation windows (e.g., 2034/6/7–2034/9/6), under a convergence criterion of $\Delta T \leq 0.005\,°\mathrm{C}$.

The key payloads do not have high-power dissipation and are well decoupled with the satellites platform. Hence, they are not included in the current simulation to save computational costs. The main material parameters used in the model are shown in Tables II and III. The primary focuses are on the effects of solar heat transfer to the satellite interior through the sunshield and top plate. The effectiveness of the thermal design is reflected, e.g., by the temperature variation of the laser unit inside the satellite.

III. SIMULATION RESULTS

Long transient thermal simulations are carried out for the thermal design aforementioned. The results of temperature variations over 3-month observation windows are obtained.

A. Sunshield temperatures

With the solar heating alone, the temperature variations of the sunlit surface (the center of $+Z$ side, see Fig. 4) span a range of 26.1–51.7 °C (see Fig. 5). In contrast, if a higher equivalent absorptivity of, e.g., 0.64 were used, the temperature variations would grow to a higher and broader range of 68.7 to 96.8 °C. This reflects the benefit of applying more OSRs.

In addition to the large variations in the β angle associated with TianQin's orbits, there is also the issue of handling excess power generated from the power subsystem. The solar array area (8.8 m^2) has been sized to meet the onboard energy consumption under the worst case scenario, i.e., the peak power (1.1 kW) at the end of life (EOL) with the photoelectric conversion efficiency η at its minimum and the β angle at 30°. This means that excess power is produced at the BOL with a higher η (~30%), and at large β angles.

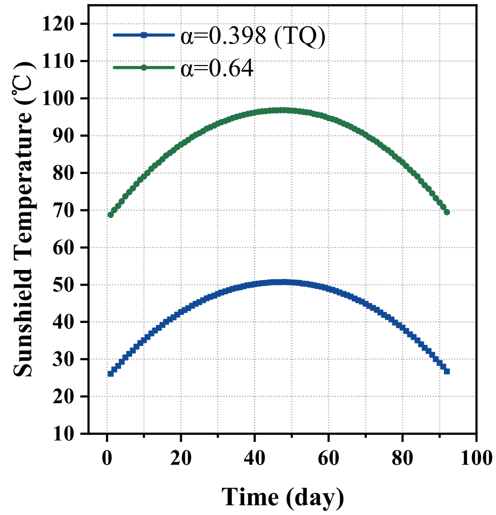

FIG. 5. Temperatures of the illuminated sunshield surface due to solar radiation alone in the first observation window, with different absorptivities.

To manage this excess power, there are two primary approaches, either dissipating it through the radiator panels as heat, or diverting the excess portion of the solar power to back the solar array to dissipate. Due to limited areas of the radiators and the concern of added thermal noises, the more viable option is the latter, i.e., to employ the sunshield itself as a radiator of the waste heat.

By imposing both the solar heat and waste heat on the illuminated surface of the sunshield, the simulation shows a temperature variation of 38.2–65.2 °C during the first observation window [see Fig. 6(a)]. It can be seen that the waste heat from the power subsystem raises the sunshield temperature by ~10 °C. Additionally, the top plate (the center of $+Z$ surface) is of 8.2–17.1 °C.

As the in-orbit observation proceeds, degradation of surface material properties leads to increased absorptivities, and a decrease in the solar cell η value results in less waste heat. The two effects partly cancel each other, and the total heat input varies less across multiple observation windows. For example, in the tenth observation window near EOL, when the absorptivity of the sunshield rises up to 0.44 and the value of η drops to 23%, the overall temperatures of the satellite slightly go up as shown in Fig. 6(b). More specifically, the illuminated surface of the sunshield shows a variation of 43.9–74.1 °C, and the top plate shows

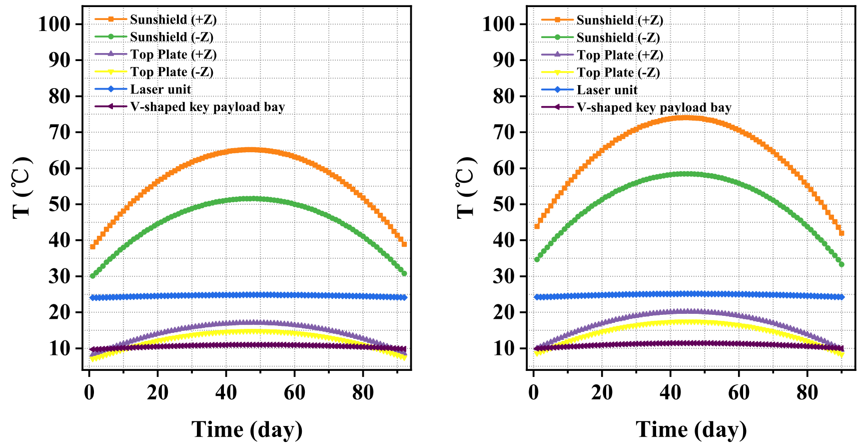

(a) Temperature variations in the first observation window

(b) Temperature variations in the tenth observation window

FIG. 6. Simulated satellite temperatures at various locations.

10.0–20.2 ℃. However, the temperature ranges of the inside equipment are less affected and stay approximately the same through the mission lifetime.

The thermal design of the sunshield encompasses three key components. The first is low absorption/high emissivity OSRs. The solar absorption (excluding the part converted to electric power) on the illuminated surface ranges from 382.5 to 527 $\mathrm{W/m^2}$, while the radiant flux (emitted infrared) ranges from 447.5 to 623.3 $\mathrm{W/m^2}$, which plays an important role in reducing the temperature of the sunshield. The second is polyimide foams with low thermal conductivity. The foams exhibit conduction flux ranging from 2.2 to 3.7 $\mathrm{W/m^2}$ at the center of the sunshield (see Fig. 7), resulting in temperature variations of 38 to 65 ℃. The third is the gap between the sunshield and the top plate, as well as the gold coating and MLI on the radiant heat transfer path. The decoupling of radiation heat results in the top plate maintaining a lower temperature compared to the interior of the satellite. Essentially, the top plate functions as a radiator, with the net flux of its upper surface ranging from -1.3 to -2.6 $\mathrm{W/m^2}$. This flux represents the difference between incident infrared and emitted fluxes of the top plate.

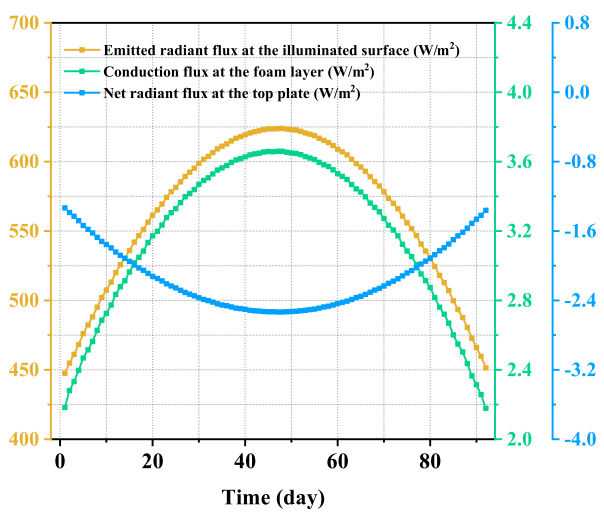

FIG. 7. Heat flow variations at the illuminated surface of the sunshield, the polyimide foam layer, and the top plate of the satellites, respectively.

B. Internal temperature variations

Analyzing the heat transfer into the satellite body, we find that the temperature variations are 7.7 ℃ for the top plate (the center of the -Z side) and 0.7 ℃ for the laser unit, respectively. Fig. 8 shows the temperature distributions inside the satellite, corresponding to the moments of the minimum and maximum solar absorption (2034/6/7 and 2034/7/22, respectively) in the first observation window. The operating temperatures of payload units such as the laser unit and the front-end electronics of the inertial sensors remain within a 1 ℃ range. On the outer surface of the V-shaped key payload bay, the temperature at the test point (see Fig. 2) varies from 9.7 to 11 ℃, with a 1.3 ℃ variation (see Fig. 6). This indicates that the design solution can create a stable thermal environment for the key payload.

C. Frequency domain analysis

The thermal design must also meet the frequency domain requirements. Here, we use a single-frequency approach for quick assessment of the effectiveness of the thermal design to attenuate temperature noise [16]. In transient analysis, a sufficiently small numerical convergence criterion (10^{-4} K) was chosen to conduct a frequency response simulation at 0.1 mHz. The amplitude spectral density of the observed SCF is given as $\tilde{S} = 1.3\times10^{-4}\cdot f^{-1/3}\cdot S_0$ $\mathrm{W/m^2/Hz^{1/2}}$ with $S_0 = 1324$ [4]. Thus, at 0.1 mHz, the fluctuation is 3.8 $\mathrm{W/m^2/Hz^{1/2}}$.

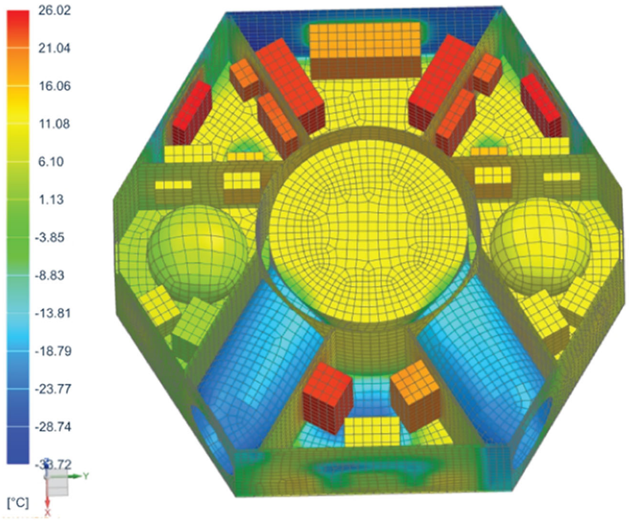

(a) satellite temperature at $\beta = 45°$

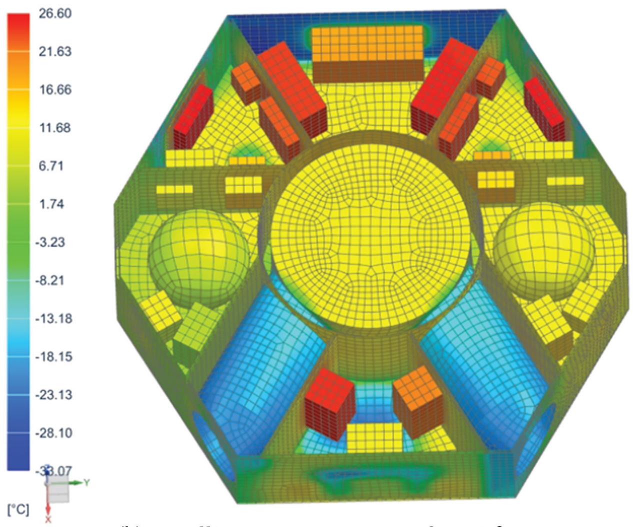

(b) satellite temperature at $\beta = 85°$

FIG. 8. Temperature distributions at the minimum and maximum β angles in the first observation window.

The solar disturbance is injected onto the sunshield as a sine wave of 0.1 mHz. The corresponding responses ($\tilde{\delta T}$) as well as the coupling factors ($\tilde{\delta T}/\tilde{S}$) at the sunshield (illuminated and bottom surfaces) and top plate ($+Z$ surface) are summarized in Table IV. The frequency 0.1 mHz is tested since the thermal noise normally goes down as the frequency f increases, making the requirement hardest to meet at the lower end of the measurement band. The results show that the temperature fluctuation from the SCF at the top plate is below the preliminary requirement of 10^{-2} K/Hz$^{1/2}$ at 0.1 mHz. Therefore, we expect that the issue of the solar flux noise can be resolved.

IV. CONCLUDING REMARKS

The paper proposes a passive thermal design for the sunshield and top plate of the TianQin satellites to mitigate the impact of external heat flow variations on the operating temperatures of the key payloads inside. Preliminary assessments show that the temperature change at the interface of the key payloads can be effectively suppressed. The results can provide a useful reference for investigating temperature-dependent effects. The key findings can be summarized as follows:

(1) The time-varying β angle introduces variations in received solar heat and also variations in waste heat from the power subsystem. On the sunshield, the ample OSR area laid among the solar cells can significantly reduce the absorbed solar heat, thereby bringing down the overall temperature of the sunshield, which varies roughly from 38 to 65 °C over three months. Therefore, both the solar heat transfer into the satellite body and its variation are diminished.

(2) By applying a combination of "polyimide foam + gold coating + MLI + aerogel" to the sunshield and top plate, the temperature range of the laser unit inside the satellite are estimated to be 24.1–24.8 °C with a variation of 0.7 °C over three months. This meets the preliminary requirement.

(3) By simulating fluctuations in the solar flux, the response of the satellite top plate registers 2.02×10^{-3} K/Hz$^{1/2}$ at 0.1 mHz. Therefore, the requirement at the top plate can be met. For future studies, more attention should be given to addressing thermal noises originating from internal electronic instruments.

It is worth noting that the thermal conductivity of polyimide foams, which assumes 0.0054 W/(m·K) ([27], and see also [4]) in this study, plays an important role in the design. The foam properties will be the subject of future studies and verification. We also point out that the temperature variations within the satellites can also be reduced by augmenting the thickness of the foams in the sunshield. Thereby, more trade studies will be carried out,

TABLE IV. Response to solar sinusoidal input at 0.1 mHz.

	Temperature response (K/Hz$^{1/2}$)	Coupling factor K/(W/m^2)
Sunshield illuminated surface	2.12×10^{-1}	5.58×10^{-2}
Sunshield bottom surface	2.98×10^{-2}	7.84×10^{-3}
Top plate $+Z$ surface	2.02×10^{-3}	5.32×10^{-4}

and the thermal design will continue to evolve though the current mission phase.

ACKNOWLEDGMENTS

The authors thank Jiajian Pan, Zening Sun, Baoxing Chen, Houyuan Chen, Ran Wei, Yanwei Ding, Hsien-Chi Yeh, Shanqing Yang, Jun Luo, and the anonymous referee for helpful discussions and comments. X. Z. is supported by the National Key R&D Program of China (Grants No. 2020YFC2201202 and No. 2022YFC2204600) and NSFC (Grant No. 12373116).

[1] J. Luo *et al.*,TianQin: A space-borne gravitational wave detector, Classical Quantum Gravity **33**, 035010 (2015).

[2] K. Danzmann, LISA: A proposal in response to the ESA call for L3 mission concepts, Technical Report, Albert Einstein Institute Hannover, 2017, https://www.semanticscholar.org/paper/LISA-Laser-Interferometer-Space-Anten na-A-proposal-Danzmann-Audley/73639f6a7d76bce4cfca3c0766c16e3596ea2bbf.

[3] B. Ye, X. Zhang, and Y. Ding, Eclipse avoidance in TianQin orbit selection, Phys. Rev. D **103**, 042007 (2021).

[4] H. Faulks, K. Gehbauer, and K. Honnen, Study of the laser interferometer space antenna (LISA)—final technical report, Technical Report No. LI-RP-DS-009, Dornier Satellitensysteme GmbH, 2000.

[5] M. van Veggel, A. Wielders, and H. van Brug, Experimental set-up for testing alignments and measurement stability of a metrology system in Silicon Carbide for GAIA, Proc. SPIE Int. Soc. Opt. Eng. **5877**, 587701 (2005).

[6] L. Page, The Wilkinson microwave anisotropy probe, Technical Report, Department of Physics, Princeton University, 2003, arXiv:astro-ph/0306381.

[7] X. Zhang, H. L. Li, and J. Mei, Thermal stability estimation of TianQin satellites based on LISA-like thermal design concept (2018), internal technical report (in Chinese).

[8] H. Chen, C. Ling, and X. Zhang, Thermal environment analysis for TianQin, Classical Quantum Gravity **38**, 155015 (2021).

[9] H. Chen, C. Ling, and Z. Yao, Thermal environment analysis for TianQin: II. Solar irradiance disparity across constellation, Classical Quantum Gravity **39**, 165009 (2022).

[10] H. Chen, Y. Ding, and J. Pan, Thermal environment analysis for TianQin: III. Low-frequency thermal transfer inside the flat-top sun shield, Classical Quantum Gravity **40**, 085001 (2023).

[11] M. Chwalla, K. Danzmann, and G. Fernández Barranco, Design and construction of an optical test bed for LISA imaging systems and tilt-to-length coupling, Classical Quantum Gravity **33**, 245015 (2016).

[12] N. A. Fishwick and N. Dunbar, In-orbit thermal control system performance results from LISA Pathfinder LEOP and Thermal Commissioning:46th International Conference on Environmental Systems (2016).

[13] M. Armano, H. Audley, and J. Baird, Temperature stability in the sub-milliHertz band with LISA Pathfinder, Mon. Not. R. Astron. Soc. **486**, 3 (2019).

[14] H. Peabody and S. Merkowitz, LISA thermal design, Classical Quantum Gravity **22**, S403 (2005).

[15] S. Merkowitz, S. Conkey, and W. Haile, Structural, thermal, optical and gravitational modelling for LISA, Classical Quantum Gravity **21**, S603 (2004).

[16] G. S. F. Center, Laser interferometer space antenna (LISA) sciencecraft description, Technical Report No. LISA-SC-DD-0001, NASA, 2009.

[17] F. Antonucci, M. Armano, and H. Audley, The LISA Pathfinder mission, Classical Quantum Gravity **29**, 124014 (2012).

[18] G. D. Racca and P. W. McNamara, The LISA Pathfinder mission, Space Sci. Rev. **151**, 159 (2010).

[19] C. Trenkel, D. Wealthy, and N. Dunbar, The engineering of LISA Pathfinder—the quietest laboratory ever flown in space, J. Phys. Conf. Ser. **840**, 012006 (2017).

[20] ESA, LISA internal final presentation, Technical Report, ESTEC, 2017.

[21] K. Chen, X. Zhang, and T. Guo, Key technologies analysis and design of ultra-clean & ultra-stable spacecraft for gravitational wave detection, Int. J. Mod. Phys. A **36**, 2140021 (2021).

[22] J. Feng, X. Zhang, and H. Liang, Key technology and experimental verification of precision thermal control of Taiji-2 satellite, J. Astronaut. **44**, 132 (2023).

[23] M. Bulut, Thermal design, analysis, and testing of the first Turkish 3U communication CubeSat in low earth orbit, J. Therm. Anal. Calorim. **143**, 4341 (2021).

[24] J. Liu, Y. Li, and D. Liu, Satellite MEMS thermal control system dynamic characteristics and autonomous thermal control strategy, Acta Aeronaut. Astronaut. Sin. **31**, 671 (2010).

[25] R. Osiander, S. L. Firebaugh, and J. L. Champion, Microelectromechanical devices for satellite thermal control, IEEE Sens. J. **4**, 525 (2004).

[26] S. Cao, X. Chen, and G. Wu, Micro louvers for micro and nano-satellites thermal control, Adv. Mater. Res. **317–319**, 1658 (2011).

[27] R. Takagi, S. Tachikawa, and T. Ohmura, Measurement and estimation of high-vacuum effective thermal conductivity of polyimide foam in the temperature range from 160, Int. J. Thermophys. **35**, 277 (2014).

[28] Y. Qin, Q. Peng, and Y. Zhu, Lightweight, mechanically flexible and thermally superinsulating rGO/polyimide nanocomposite foam with an anisotropic microstructure, Nanoscale Adv. **1**, 4895 (2019).

[29] W. Fan, X. Zhang, and Z. Y, Lightweight, strong, and super-thermal insulating polyimide composite aerogels under high temperature, Compos. Sci. Technol. **173**, 47 (2019).

[30] X. Yue, H. Wu, and T. Zhang, Superhydrophobic waste paper-based aerogel as a thermal insulating cooler for building, Energy **245**, 123287 (2022).
[31] R. Wordsworth, L. Kerber, and C. Cockell, Enabling martian habitability with silica aerogel via the solid-state greenhouse effect, Nat. Astron. **3**, 898 (2019).
[32] H. Mesforoush, M. R. Pakmanesh, and H. Esfandiary, Experimental and numerical analyses of thermal performance of a thin-film multi-layer insulation for satellite application, Cryogenics **102**, 77 (2019).
[33] A. V. Nenarokomov, L. A. Dombrovsky, and I. V. Krainova, Identification of radiative heat transfer parameters in multilayer thermal insulation of spacecraft, Int. J. Numer. Methods Heat Fluid Flow **27**, 598 (2016).
[34] C. Sun, H. F. Sun, and Z. Y. Wang, Experiment and analysis on radiation properties of SiO_2/Ag optical solar reflector coating, Aerosp. Sci. Technol. **82–83**, 372 (2018).
[35] T. Liu, Q. Sun, and J. Meng, Degradation modeling of satellite thermal control coatings in a low earth orbit environment, Solar Energy **139**, 467 (2016).
[36] R. P. Kornfeld, B. W. Arnold, M. A. Gross, N. T. Dahya, W. M. Klipstein, P. F. Gath, and S. Bettadpur, GRACE-FO: The gravity recovery and climate experiment follow-on mission, J. Spacecr. Rockets **56**, 931 (2019).